On the validity of periodic boundary conditions for modelling finite plate-type acoustic metamaterials

Felix Langfeldt[1, a]

Institute of Sound & Vibration Research, University of Southampton, University Road, Highfield, Southampton, SO17 1BJ, United Kingdom

(Dated: 7 January 2024)

Plate-type acoustic metamaterials (PAM) are thin structures that exhibit anti-resonances with high sound transmission loss values, making PAM a promising new technology for controlling tonal noise in the challenging low-frequency regime. A PAM consists of rigid masses periodically attached to a thin baseplate. The periodicity of PAM can be exploited in simulations allowing to model only a single unit cell using periodic boundary conditions. This approach essentially represents the PAM as an infinite structure, but real PAM implementations will always be finite and influenced by boundary conditions. In this paper, extensive numerical simulations of different PAM configurations have been performed to study the performance of finite PAM compared to infinite PAM. The results indicate that as the number of unit cells in a finite PAM increase, the sound transmission loss converges towards that of an infinite PAM. The impact of the finite PAM edge boundary conditions becomes negligible at some point. Based on the numerical results, a simple criterion is proposed to determine a-priori how many unit cells are required in a finite PAM design to consider it quasi-infinite. This criterion aids in justifying unit cell models with periodic boundary conditions for efficient design optimizations in practical PAM applications.

[a]F.Langfeldt@soton.ac.uk

I. INTRODUCTION

Since more than 20 years, acoustic metamaterials have been widely studied as an emerging technology to control the propagation of sound waves in many different and previously unheard of ways (Cummer *et al.*, 2016; Ma and Sheng, 2016). One particular strength of acoustic metamaterials, which caught the attention of the noise control research community, is that they can be used to control low-frequency tonal noise using very thin and lightweight structures (Gao *et al.*, 2022). Of the many acoustic metamaterial types that have been proposed in the past, plate-type acoustic metamaterials (PAM) are plate-like structures, consisting of a thin baseplate and periodic subwavelength sized unit cells containing rigid masses which are attached to the baseplate. Figure 1 shows an example of a PAM with one annular mass in each unit cell. The basic design of PAM is very similar to that of membrane-type acoustic metamaterials (MAM), which use a pre-stressed membrane as the baseplate (Yang *et al.*, 2010, 2008). The key advantage of PAM over MAM is that the stiffness of the baseplate in PAM does not depend on a pre-stress and therefore the acoustical properties of PAM are more robust with respect to stress relaxation and temperature effects and PAM do not require a rigid (and heavy) grid structure to support the pre-stress (Huang *et al.*, 2016; Ma *et al.*, 2021).

Previous research has demonstrated that PAM can exhibit frequency bands at low frequencies (typically below 1 kHz) with sound transmission loss (STL) values greatly exceeding the STL of a homogeneous wall with the same mass, which is governed by the mass-law (Langfeldt and Gleine, 2019; Xiao *et al.*, 2021). These high STL frequency bands are asso-

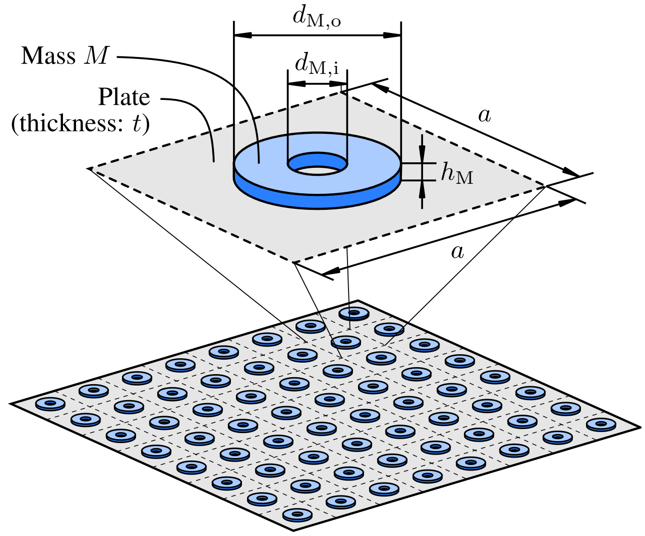

FIG. 1. Geometry of a finite PAM with annular added masses and 8×8 unit cells. The geometry of an individual unit cell is shown at the top.

ciated with the anti-resonances of the PAM, i.e. frequencies at which the surface-averaged displacement of a unit cell is zero for a given acoustic excitation and the PAM acts like an (almost) rigid wall to incident sound waves (Yang *et al.*, 2008). The high STL of PAM combined with their low mass and thickness makes PAM a promising solution for low-frequency noise control problems, especially in applications where weight and space are highly constrained (e.g. in the aeronautical or automotive industries). Due to these appealing properties, a number of studies on the sound insulation of PAM have been published in the past, including experimental investigations of large-scale samples in the laboratory (Langfeldt and Gleine, 2020a; Xiao *et al.*, 2021) and analytical models (Langfeldt and Gleine, 2019). As is common for the modelling of metamaterials in general, most numerical and analytical studies of PAM used a model of a unit cell with periodic boundary conditions to predict the vibro-acoustic properties of PAM (Langfeldt and Gleine, 2019; Xiao *et al.*, 2021). This approach essentially idealizes the PAM as an unbounded metasurface with an infinite number of unit cells. This approach has a number of advantages, for example it is very computationally efficient as only a single unit cells needs to be modelled and it enables the use of homogenization methods (Yang *et al.*, 2014).

Real structures, however, are always finite-sized and it is possible that the boundary conditions of finite PAM structures can lead to deviations from the idealized periodic unit cell model. As a noteworthy example, Sui *et al.* (2015) investigated the STL of a honeycomb-type acoustic metamaterial with a surface mass density of $1.3\,\mathrm{kg\,m^{-2}}$ using measurements in an impedance tube. Despite the low weight of the metamaterial, they observed STL values of over 45 dB at frequencies below 500 Hz. However, as pointed out by Peiffer *et al.* (2015), this result was due to the impedance tube sample being small (diameter 100 mm) with fixed edges and therefore its low-frequency STL was governed by a stiffness-controlled behavior. If the sample size would be scaled up to much higher and more practical values (e.g. $1\,\mathrm{m^2}$), the STL of the metamaterial would be simply governed by the mass-law and STL values of 45 dB could not be reached below 500 Hz (Peiffer *et al.*, 2015). Varanasi *et al.* (2017) presented experimental results for a finite multi-celled PAM-like metamaterial plate, consisting of a thin plate with a rectangular grid and a sound normalizing layer. They compared their experimental results to unit cell-based numerical simulations (Varanasi *et al.*, 2013) and discovered deviations between the measured and simulated frequency of the metamaterial's STL peak, which they attributed to the different behavior of the finite metamaterial in the experiment and the infinite metamaterial in the simulation. In a different investigation, Van Belle *et al.* (2019) studied the STL of infinite and finite vibro-acoustic metamaterial plates consisting of mechanical resonators or point masses periodically attached to a host plate. In their results, the authors could show that the infinite metamaterial plate with point masses (which exhibits similar characteristics as the PAM considered in this work) exhibits an anti-resonance with large STL values, whereas in the finite case with 12 $\times$ 9 unit cells the anti-resonance STL values were significantly reduced by the eigenmodes of the finite structure.

Although the studies mentioned above indicate that the performance of a finite sized PAM can be very different compared to an idealized unit cell model with periodic boundary conditions, there exist other numerical and even experimental results for the STL of finite PAM which show a good agreement with predicted anti-resonance frequencies and STL values from periodic unit cell representations (Langfeldt and Gleine, 2020a; Xiao *et al.*, 2021). It is still unknown under which circumstances finite acoustic metamaterial plates can be modelled using unit cells with periodic boundary conditions. To fill this gap, this paper presents the results of systematic numerical simulations of finite PAM with different numbers of unit cells to study the impact of the PAM boundary conditions on the STL, as compared to the STL of an infinite PAM. The aim is to develop a criterion which can be used to estimate if a finite PAM design is large enough to be represented by a periodic unit cell model with sufficient accuracy. Such a criterion will give more confidence in the design of practical PAM for noise control and can be used to justify the choice of a modelling approach using periodic unit cells. Section II of this paper provides a detailed description of the simulation model that was used in this study to investigate the properties of finite PAM with different numbers of unit cells. Simulations have been performed for two different

PAM designs and the numerical results for the sound transmission loss and the finite PAM anti-resonances are presented in section III. These results are then discussed in section IV and further analysed to develop a simple criterion for assessing the suitability of a unit cell with periodic boundary conditions to represent a finite PAM with a certain number of unit cells. At the end of this section, this criterion is validated using a PAM test case study. Finally, the results presented in this paper are summarized and concluded in section V.

II. NUMERICAL MODEL

Numerical simulations based on the finite element method (FEM) are used to calculate the normal incidence STL of different finite sized PAM. In this work, the normal incidence STL was simulated to minimize the computational cost, especially for the finite PAM models with large numbers of unit cells. For normal incidence the STL needs to be simulated only for a single incidence acoustic loading (as compared to integrating the STL over a range of incidence angles for diffuse incidence STL). Additionally, the symmetry of normally incident plane waves and the PAM itself makes it possible to model only a quarter of the PAM and the fluid domains (as shown in Figure 2). It has been shown in previous investigations that the anti-resonance frequencies of PAM are the same for normal and diffuse incidence (Langfeldt and Gleine, 2019), which justifies this approach for the aim of this study. Figure 2(a) provides an overview of the dimensions and boundary conditions of the numerical model. The PAM was embedded inside a rigid infinite baffle. Unless stated otherwise, the exterior edge of the PAM, where the PAM meets the baffle, was constrained using simply supported boundary conditions. The acoustic excitation of the PAM was performed by imposing a spatially constant pressure amplitude $p_{\mathrm{bl}} = 2p_{\mathrm{in}}$ on the PAM, which corresponds to the blocked pressure field generated by a normally incident plane acoustic wave with amplitude p_{in}. To obtain the radiated sound field, one side of the PAM was coupled to a fluid half space, as shown in Figure 2(a), via a full vibro-acoustic coupling condition. The transmitted sound power W_{tr} was obtained by integrating the surface-normal component of the acoustic intensity on the fluid-PAM interface. With the incident sound power of the incident plane wave given by $W_{\mathrm{in}} = S\,|p_{\mathrm{in}}|^2/(2\rho_0 c_0)$, where $S = N^2a^2/4$ is the area of the quarter model of the PAM and $\rho_0 = 1.2\,\mathrm{kg\,m^{-3}}$ and $c_0 = 340\,\mathrm{m\,s^{-1}}$ are the density and the speed of sound of the fluid, respectively, the STL can be obtained via $\mathrm{TL} = -10\lg(W_{\mathrm{tr}}/W_{\mathrm{in}})$.

The PAM itself was modelled using shell elements with quadratic Lagrange basis functions for the baseplate and solid elements with quadratic serendipity basis functions for the added masses. The materials were modelled as linear elastic materials including damping using a structural loss factor η. An overview of the density ρ, Young's modulus E, Poisson's ratio ν, and loss factor η for the materials used in this study is provided in Table I. For the air domain, fluid elements with quadratic Lagrange basis functions were used. The maximum element size was set to 56.7 mm, corresponding to at least six elements per wavelength at the highest frequency of interest 1000 Hz. To sufficiently resolve the curved regions at the edges of the added masses of the PAM, the maximum element size was set to 20 % of the curvature radius of these edges. On the baseplate, a triangular mesh was used to discretize the shell. Then, the masses were discretized using a swept mesh with one element thickness. A tetrahedral mesh was then generated in the radiation fluid domain. Finally, perfectly matched layers (PML) were added to truncate the fluid domains and simulate

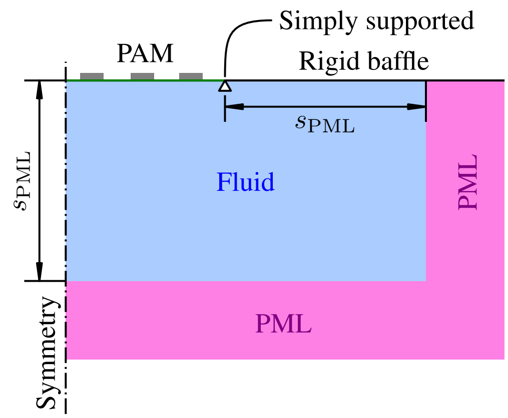

(a)

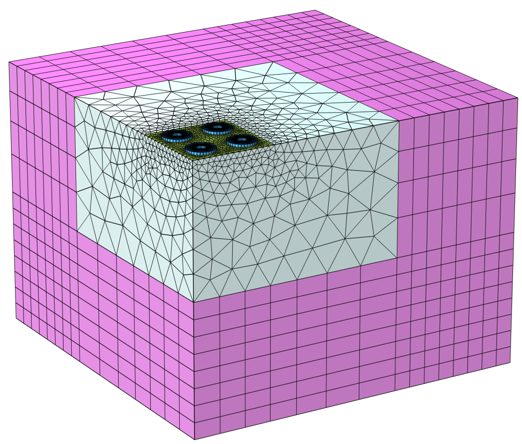

(b)

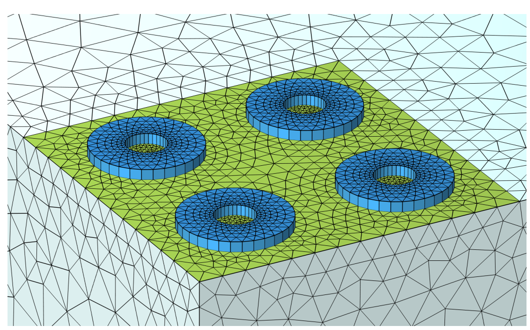

(c)

FIG. 2. Numerical setup for calculating the normal incidence STL of finite sized PAM. (a) Dimensions and boundary conditions; (b) Overview of the mesh of the whole simulation model for configuration PAM2 with 4×4 unit cells; (c) Detail view of the PAM mesh.

TABLE I. Material properties of the materials used in the numerical simulations.

Material name	ρ	E	ν	η
Steel	7850	205	0.28	1
Polycarbonate (PC)	1310	2.3	0.4	5
Polyamide	1150	2.9	0.4	5
Polyethylene terephthalate (PET)	1400	4.5	0.4	5
	$\mathrm{kg\,m^{-3}}$	GPa	—	%

the sound radiation into a half space. $N_{\mathrm{PML}} = 8$ layers in the PML regions were found to sufficiently suppress the reflection of sound waves across the whole frequency range of interest. The distance between the PML and the PAM, as indicated in Figure 2(a), was set to $s_{\mathrm{PML}} = 70.8\,\mathrm{mm}$, corresponding to 1/48 of the wavelength at the lowest frequency of interest (100 Hz). An example of the mesh generated for PAM configuration PAM2 (see Table II) with 4×4 unit cells is shown in Figure 2(b) and Figure 2(c). To ensure that the PML setup and the discretization did not affect the simulation results significantly, additional parametric and mesh convergence studies have been performed. The interested reader can find these results in the Supplementary Materials.[1]

TABLE II. Simulated PAM unit cell configurations.

						Materials			
Configuration	a	t	$d_{\mathrm{M,o}}$	$d_{\mathrm{M,i}}$	h_{M}	Baseplate	Masses	$f_{\mathrm{P}\infty}$	m''
PAM1	77.5	750	30	0	1	PC	Steel	252	1.9
PAM2	22.5	50	14.7	5.4	1.4	PET	Polyamide	294	0.54
	mm	µm	mm	mm	mm			Hz	$\mathrm{kg\,m^{-2}}$

III. RESULTS

In this section, the results of the numerical simulations of finite and infinite PAM configurations will be presented. Two different PAM unit cell configurations, denoted PAM1 and PAM2 with details provided in Table II, will be compared. PAM1 corresponds to the design that was studied numerically and experimentally in Langfeldt and Gleine (2020a), whereas configuration PAM2 represents a more lightweight design with smaller unit cells compared to PAM1. The presentation of the results in this section will first focus on the comparison of sound transmission loss spectra for different finite and infinite PAM configurations. Then, results for the finite PAM anti-resonances versus the number of unit cells will be presented for different PAM edge boundary conditions.

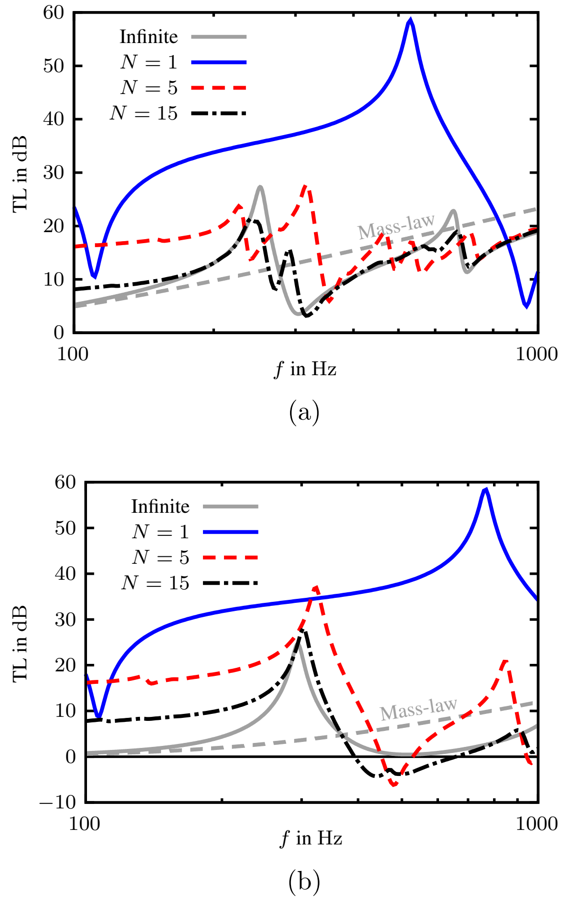

FIG. 3. Simulated sound transmission loss of the finite and infinite PAM. The grey dashed curve represents the mass-law STL using the static surface mass density of the PAM m''. (a) PAM1; (b) PAM2.

A. Sound transmission loss

Figure 3(a) and Figure 3(b) show the simulated sound transmission loss of PAM1 and PAM2, respectively, for increasing number of unit cells $N \times N$. Additionally, both plots contain the STL of the infinite PAM (grey solid curve), simulated using a unit cell with periodic boundary conditions, and the mass-law STL (grey dashed curve) as a reference. It should be noted that in Figure 3(b) some frequency ranges with negative STL values can be seen. This result is not unphysical, but merely a result of the small size of the PAM panels (the unit cells of PAM2 are three times smaller than the PAM1 unit cells), the presence of diffraction around the panel edges, and the definition of the incident sound power, as discussed by Thompson *et al.* (2009).

In both cases shown in Figure 3 it can be observed that if just a single unit cell is considered, then the anti-resonance occurs at a much higher frequency than in the infinite periodic case. This is not unexpected, since the simply supported boundary conditions impose a stiffness to the PAM unit cell, leading to the increase in frequency. Furthermore, the STL values of the $N = 1$ finite PAM generally are much higher than in the infinite case, which is a result of the spatial windowing effect (Villot *et al.*, 2001). As N is increased, it can be seen in both the results for PAM1 and PAM2 that the general STL values of the finite PAM decrease (due to the finite panels becoming larger, leading to a reduction of the spatial windowing effect) and the anti-resonance approaches the corresponding anti-resonance frequency of the infinite PAM. An explanation for this is that as the number of unit cells increases, a decreasing proportion of unit cells within the finite panel are affected by the exterior boundary conditions. In the limit $N \to \infty$, no unit cells are constrained by the simply supported boundary conditions and the periodic boundary conditions assumed in the infinite PAM model are valid.

A significant difference between the finite STL values of PAM1 and PAM2 for increasing N is that in the case of PAM1 and $N = 5$ two STL peaks appear next to the infinite PAM anti-resonance with a resonance dip in between. These two peaks and the dip are still visible for $N = 10$, only with slightly shifted frequencies. In case of PAM2, however,

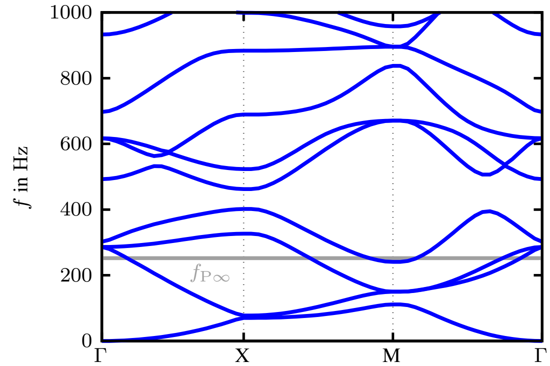

(a)

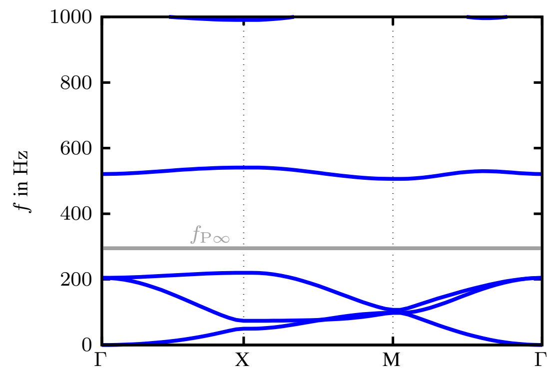

(b)

FIG. 4. Dispersion curves of the PAM unit cells. The grey horizontal line denotes the anti-resonance frequency $f_{\mathrm{P}\infty}$ of the infinite PAM. (a) PAM1; (b) PAM2.

there is just one dominant anti-resonance peak which steadily approaches the infinite PAM anti-resonance as N is increased. The explanation for the larger number of peaks in the finite PAM1 configuration can be found in the dispersion curves of the metamaterial, shown in Figure 4. For PAM1, the infinite PAM anti-resonance frequency $f_{\mathrm{P}\infty}$ does not coincide with a band-gap and therefore the anti-resonance of the finite PAM is disturbed by the presence of structural modes (Van Belle *et al.*, 2019). In case of PAM2, $f_{\mathrm{P}\infty}$ falls within a fairly large complete band-gap and thus the finite PAM STL curves are much smoother.

It should be noted that for a PAM the anti-resonance (with high STL values) does not necessarily fall within a bending wave band-gap of the metamaterial. As evident from the dispersion curves in Figure 4 as well as by comparing the band-gap frequencies with the STL curves in Figure 3, this depends on the design of the PAM unit cell. This is because the band-gap in PAM is governed by Bragg interference effects, because the added masses act as periodic non-resonant scatters, whereas the anti-resonance frequency depends on the first few eigenmodes of the unit cell (Langfeldt and Gleine, 2020b; Yang *et al.*, 2008). Van Belle *et al.* (2019) provide further insights on the band-gaps and anti-resonances of metamaterial plates with resonant and non-resonant scatterers.

B. Anti-resonance

Figure 5(a) shows the anti-resonance frequency f_{P} of configuration PAM1 for increasing number of unit cells $N = 1 \ldots 30$ and two different boundary conditions for the PAM edges (simply supported and clamped). Note that, as observed in Figure 3, for some finite PAM configurations multiple peaks can appear in the STL spectrum, even though the unit cell has been designed to exhibit only one anti-resonance frequency. Thus, f_{P} has been defined in the finite PAM cases as the frequency corresponding to the largest STL maximum in the investigated frequency range. The results in Figure 5(a) indicate that for very low number of unit cells ($N \leq 6$), the anti-resonance frequency of the finite PAM1 is much higher than the infinite PAM anti-resonance frequency $f_{\mathrm{P}\infty} = 252\,\mathrm{Hz}$. This is because the boundary conditions of the PAM increase the stiffness of the unit cells globally, leading to a shift to higher frequencies. As the number of unit cells becomes larger, the finite PAM

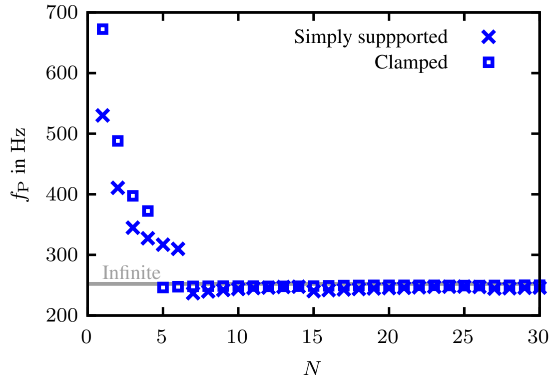

(a)

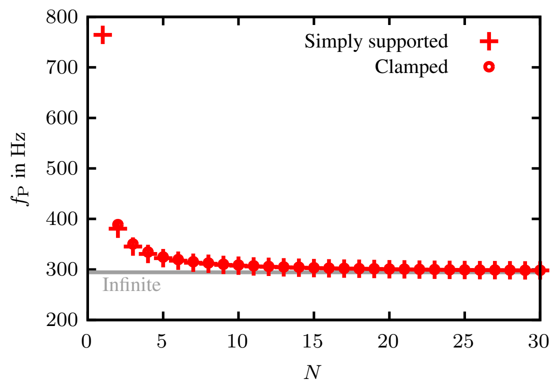

(b)

FIG. 5. Anti-resonance frequency of the finite PAM for different number of unit cells $N \times N$ and simply supported and clamped boundary conditions for the finite PAM edge. (a) PAM1; (b) PAM2.

anti-resonance frequency converges towards the infinite PAM value and the influence of the boundary conditions becomes negligible, as evident by the small differences between the simply supported and clamped PAM for larger values of N. What stands out in Figure 5(a) is that the convergence behavior of the PAM anti-resonance frequency with respect to N is not monotonic, with, in the simply supported case for example, f_P being higher than the infinite PAM anti-resonance frequency for $N \leq 6$ whereas for $N > 6$ f_P approaches $f_{P\infty}$ from lower frequencies. This non-monotonic convergence behavior is caused by different

STL peaks growing, shrinking, and changing their frequencies as the number of unit cells is increased (see Figure 3(a)). Contrary to this, the convergence behavior in case of PAM2 shown in Figure 5(b) is strictly monotonic. Since PAM2 was designed to have an anti-resonance frequency within a complete band-gap (whereas PAM1 was designed not to), this much cleaner convergence behavior can be attributed to the lack of structural modes around the anti-resonance frequency of PAM2.

Figure 6 shows the convergence behavior of the peak sound transmission loss $\mathrm{TL_P}$, defined as the STL value at the anti-resonance frequency f_P, for both finite PAM configurations. In both cases it can be seen that the $\mathrm{TL_P}$ values are much higher than for the infinite PAM if the number of unit cells is low. As discussed above, this can be attributed to the spatial windowing effect, which leads to strongly increased STL values if the finite panels are significantly smaller than the wavelength. For increasing N, the $\mathrm{TL_P}$ values converge towards the corresponding value of the infinite PAM. The convergence behavior in the case of PAM1 (Figure 6(a)) is quite irregular, similarly to what was observed for the anti-resonance frequency. The peak STL values fall slightly below the infinite PAM $\mathrm{TL_P}$ value. This can, again, be explained by the anti-resonance frequency of PAM1 not falling within a band-gap, thus the peak STL values are affected by the eigenmodes of the finite PAM. It is worth noting that for PAM1 with clamped boundary conditions, $\mathrm{TL_P}$ is much closer to the infinite value at larger N. This is because the anti-resonance of the clamped PAM1 is not so strongly disturbed by PAM eigenmodes as in the simply supported case.[2] For PAM2 (Figure 6(b)), $\mathrm{TL_P}$ decreases monotonically towards the infinite PAM value as the number of unit cells is increased. The boundary conditions have almost no effect on $\mathrm{TL_P}$. This highlights again

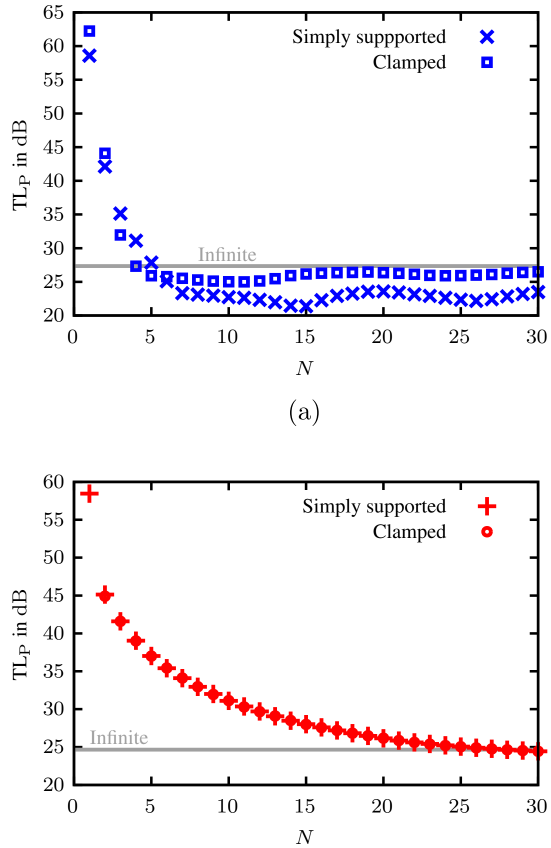

(a)

(b)

FIG. 6. Peak sound transmission loss value at the anti-resonance frequency of the finite PAM for different number of unit cells $N \times N$ and simply supported and clamped boundary conditions for the finite PAM edge. (a) PAM1; (b) PAM2.

that it is advantageous to design a finite PAM to have an anti-resonance frequency that falls within a band-gap.

IV. DISCUSSION

In this section, the results presented in the previous section will be used to develop a simple criterion for assessing the suitability of a unit cell-based numerical model with periodic

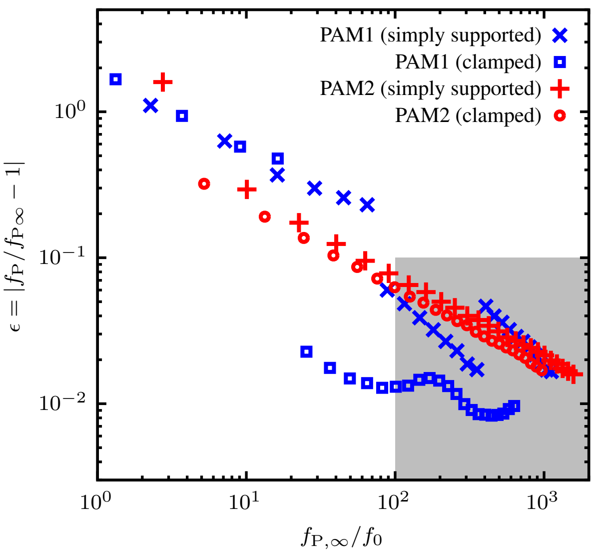

FIG. 7. Relative anti-resonance frequency error ϵ of the finite PAM with different boundary conditions and numbers of unit cells. The grey area indicates the range of values for $f_{\mathrm{P}\infty}/f_0$ at which the error is less than 10 %.

boundary conditions to predict the STL properties of a finite PAM. Then, this criterion will be applied to a new PAM design to verify the validity of the proposed approach.

A. Quasi-infinite PAM criterion

To unify the results from the previous section and identify a criterion for the minimum number of unit cells $N \times N$ for which a finite PAM is reasonably well represented using a unit cell with periodic boundary conditions, Figure 7 shows the relative error $\epsilon = |f_{\mathrm{P}}/f_{\mathrm{P}\infty} - 1|$ of the finite PAM anti resonance frequency (compared to the infinite PAM anti-resonance frequency) against $f_{\mathrm{P}\infty}$ normalized by the fundamental resonance frequency of the finite PAM f_0. f_0 was obtained from an eigenfrequency analysis of the FEM model of the PAM. Choosing $f_{\mathrm{P}\infty}/f_0$ as the measure for the error was motivated by the following reasons: As discussed above, the boundary conditions of a finite PAM affect the dynamic behavior of the PAM globally, mainly by stiffening the unit cells, leading to altered anti-resonance frequencies f_{P}. The "global stiffness" of the finite PAM is related to its fundamental resonance frequency f_0: For PAM with a very small number of unit cells, f_0 can be very large, whereas as $N \to \infty$, f_0 will approach zero. Thus, the hypothesis is that if $f_0 \ll f_{\mathrm{P}\infty}$ (and the ratio $f_{\mathrm{P}\infty}/f_0$ is very large), the influence of the finite PAM edge boundary conditions on the anti-resonance should be small.

The results Figure 7 confirm this hypothesis indicating for all considered PAM and boundary condition combinations a similar trend in the reduction of the anti-resonance frequency error ϵ as $f_{\mathrm{P}\infty}/f_0$ is increased. The grey area in Figure 7 highlights the region in which $\epsilon < 10\,\%$ consistently for all combinations of PAM designs and boundary conditions. From this, a criterion for a quasi-infinite PAM with an anti-resonance frequency less then $10\,\%$ different from the infinite PAM anti-resonance frequency can be deduced:

$$f_0 < 0.01 f_{\mathrm{P}\infty}, \tag{1}$$

i.e. the fundamental frequency of the finite PAM must be at least 100 times smaller than the desired anti-resonance frequency $f_{\mathrm{P}\infty}$.

For a useful a-priori estimation of the quasi-infinite PAM criterion, an estimation of the fundamental resonance frequency f_0 of the finite PAM for different N without requiring numerical eigenfrequency studies of the full size panel is needed. For the sake of simplicity, it is assumed here that for $N \gg 1$ the global bending wavelength at f_0 is larger than the unit cell size and thus the low-frequency behavior of the finite PAM is well represented by the smeared mass and stiffness of the inhomogeneous PAM structure (Cremer *et al.*, 2005). Thus, approximate expressions for the fundamental resonance frequency of a square homogeneous plate will be used to predict f_0 here, with

$$f_0(N) \approx \frac{\pi}{N^2 a^2}\sqrt{\frac{\overline{D}}{m''}} \tag{2}$$

for simply supported boundary conditions and

$$f_0(N) \approx 1.84\frac{\pi}{N^2 a^2}\sqrt{\frac{\overline{D}}{m''}} \tag{3}$$

for clamped boundary conditions (Ventsel and Krauthammer, 2001). In both equations, a corresponds to the unit cell size, m'' is the static surface mass density of the PAM, and $\overline{D}$ is the smeared bending stiffness. $\overline{D}$ depends on the bending stiffness of the baseplate,

$$D = \frac{Et^3}{12(1-\nu^2)}, \tag{4}$$

and the mass,

$$D_{\mathrm{M}} = \frac{E_{\mathrm{M}} h_{\mathrm{M}}^3}{12(1-\nu_{\mathrm{M}}^2)} \tag{5}$$

(assuming masses with constant thickness h_{M}), as well as the specific arrangement of the masses within the unit cell. If the mass is very small compared to the overall unit cell size (point-like), $\overline{D}$ should be very close to the baseplate bending stiffness D. For larger masses, the rigidity of the mass will stiffen the baseplate and $\overline{D}$ will be expected to be higher than D. To estimate $\overline{D}$ for added masses which are not point-like, the following rule of mixture, analogous to the modelling of composite materials, will be used:

$$\overline{D} \approx \left(\frac{\phi}{D_{\mathrm{M}}} + \frac{1-\phi}{D}\right)^{-1}, \tag{6}$$

where $\phi = 0.25\pi(d_{\mathrm{M,o}}^2 - d_{\mathrm{M,i}}^2)/a^2$ is the relative area covered by the mass in the unit cell.

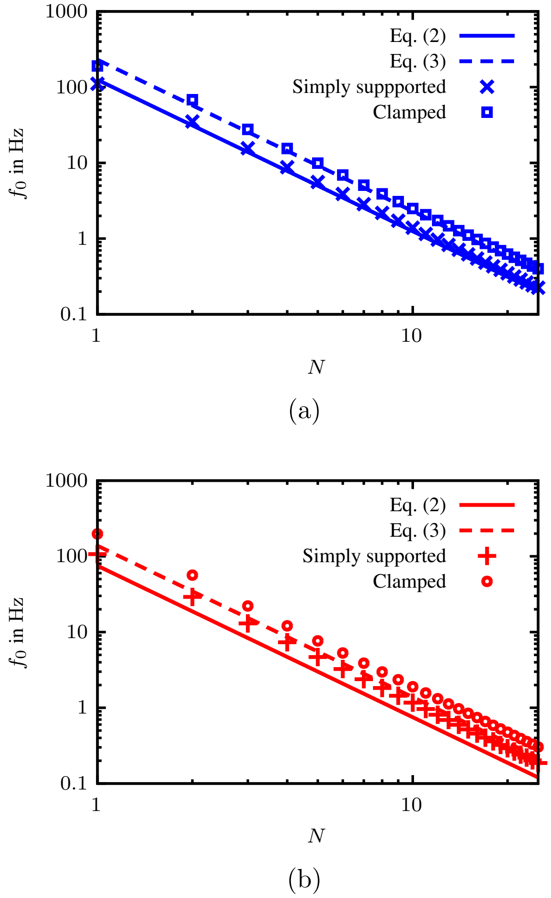

FIG. 8. Fundamental resonance frequency of the finite PAM for different number of unit cells $N \times N$ and simply supported and clamped boundary conditions for the finite PAM edge. (a) PAM1; (b) PAM2.

To evaluate the accuracy of Equation 2 and Equation 3, Figure 8 compares these estimations to the simulated fundamental frequencies of the finite PAM at different values of N. For PAM1, shown in Figure 8(a), Equation 2 and Equation 3 combined with the estimate for $\overline{D}$ in Equation 6 provide a reasonably accurate prediction of the finite PAM fundamental frequency, given the simplicity of the equations. For PAM2 in Figure 8(b) it can be seen that the model tends to underpredict the fundamental resonance frequency, for both simply supported and clamped boundary conditions. Since for PAM2 the mass size, compared to the unit cell size, is fairly large ($\phi = 29\,\%$), Equation 6 appears to underestimate the stiffening effect of the added mass. If a more accurate prediction of $\overline{D}$ is required, eigenfrequency simulations can be performed for, e.g., $N = 1$ to obtain $f_0(1)$ and Equation 2 or Equation 3 can then be solved for $\overline{D}$.

B. Application to a new PAM design

The quasi-infinite PAM criterion is now validated by applying it to a new PAM design which differs from the two designs PAM1 and PAM2 that were used to derive the criterion. The unit cell of this design, denoted PAM3, is shown in Figure 9(a). The unit cell contains a square shaped steel mass that is attached to a 100 µm thick PET baseplate. The dimensions of the mass and the unit cell are given in Figure 9(a). The different mass shape was chosen to test the robustness of the quasi-infinite PAM criterion with respect to mass shapes other than circular or annular. The dimensions and materials of the PAM3 design result in a static surface mass density of $m'' = 3.6\,\mathrm{kg\,m^{-2}}$, a smeared bending stiffness of $\overline{D} = 0.8\,\mathrm{N\,mm}$ (according to Equation 6), and an infinite PAM anti-resonance frequency of $f_{\mathrm{P}\infty} = 218\,\mathrm{Hz}$. Using these parameters and choosing simply supported boundary conditions for the finite PAM, Equation 2 is used in conjunction with the criterion in Equation 1 to determine that at least 4×4 unit cells have to be used in the finite PAM configuration to achieve an anti-resonance frequency within $\pm 10\,\%$ of $f_{\mathrm{P}\infty} = 218\,\mathrm{Hz}$.

Numerical simulation results of the STL of the infinite and finite PAM3 with $N = 4$ are shown in Figure 9(b). The grey shaded area indicates the frequency range within $\pm 10\,\%$ of

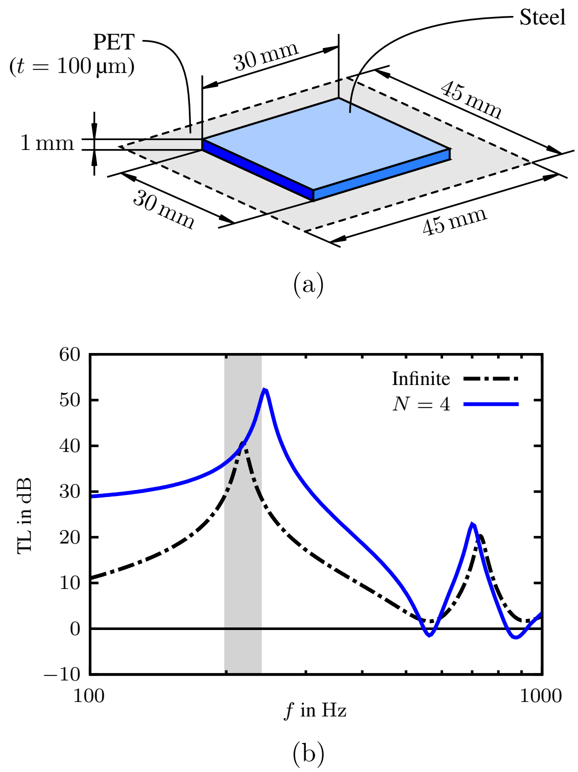

FIG. 9. (a) Unit cell design parameters for PAM3, which was used to validate the proposed quasi-infinite PAM criterion; (b) Sound transmission loss of the infinite and finite PAM3. The grey area denotes a deviation of $\pm 10\,\%$ from the infinite PAM anti-resonance frequency.

$f_{\mathrm{P}\infty}$. It can be seen that the anti-resonance peak of the finite PAM falls just outside the area. Thus, the quasi-infinite PAM criterion underestimated the necessary number of unit cells for this particular PAM design, but only by a very small margin. As discussed in the previous sub-section, the accuracy could be improved by estimating $\overline{D}$ using a simulation of the unit cell with simply supported boundary conditions. Given the simplicity of the criterion and the fact that the PAM3 unit cell design used a different mass shape than PAM1 and PAM2, the proposed criterion in Equation 1 and the smeared bending stiffness estimation in Equation 6 appear to be a useful tool for judging the appropriateness of predicting the anti-resonance frequency of a finite PAM using a unit cell model with periodic boundary conditions.

V. CONCLUSION

In the present paper the sound transmission loss of finite PAM was investigated, with particular focus on the anti-resonance frequency of the finite PAM and a comparison to the infinite PAM anti-resonance frequency. For this purpose, a large number of numerical simulations for two different PAM configurations have been performed. The results were analysed and a simple criterion to determine how many unit cells are necessary for a finite PAM so that its anti-resonance frequency differs from the infinite PAM anti-resonance frequency by less then 10 %. The key results of this study are as follows:

- The anti-resonance of a finite PAM converges towards the infinite PAM anti-resonance as the number of unit cells increases. This convergence behaviour is independent of the PAM edge boundary conditions (simply supported or clamped).

- As already shown by Van Belle *et al.* (2019) for PAM with point masses and confirmed in this study for PAM with more general mass shapes, it is advantageous to design PAM such that the anti-resonance frequency (of the infinite PAM) lies within a complete bending wave band-gap. If the PAM anti-resonance frequency does not coincide with a band-gap, peaks and dips from the resonant behaviour of the finite PAM will affect the STL spectrum around the anti-resonance frequency.

- A quasi-infinite PAM criterion has been developed and is given in Equation 1. This criterion is defined as the required fundamental resonance frequency f_0 of the finite PAM so that the finite PAM anti-resonance frequency f_{P} differs from the infinite PAM anti-resonance frequency by less then $10\,\%$.

- Equation 2 and Equation 3 can be used as simple formulas to estimate f_0 of a finite PAM and calculate the required number of unit cells N to satisfy the quasi-infinite PAM criterion.

These results will support the application of PAM in practical noise control problems. First, the simulation results confirm that computationally efficient unit cell simulation models with periodic boundary conditions provide indeed a good representation of a more realistic finite PAM with edge boundary conditions, if the number of unit cells N is large enough. Secondly, the quasi-infinite PAM criterion—though simple and therefore not highly accurate—has been proven as a useful tool to estimate, without the need for costly finite PAM simulations, if a finite PAM with a given number of unit cells can be regarded as infinite, justifying more efficient computations and enabling faster design iterations or optimizations. The PAM configurations that were considered in this study consisted of unit cells with a single mass, therefore exhibiting a single isolated anti-resonance frequency. The findings in this contribution can, however, be extended towards more advanced PAM designs with multiple anti-resonances or higher bandwidth, as long as these PAM designs can be represented using periodic unit cells, e.g. PAM with multiple masses per unit cell (Langfeldt and Gleine, 2020b) or sub-unit cells with synergetic coupling (Ma *et al.*, 2017; Wang *et al.*, 2019).

VI. SUPPLEMENTARY MATERIAL

See supplementary material at [URL will be inserted by AIP] for the results of the mesh and PML convergence study for the numerical model, as well as further STL results for PAM1 and PAM2.

ACKNOWLEDGMENTS

The author acknowledges the use of the IRIDIS High Performance Computing Facility, and associated support services at the University of Southampton, in the completion of this work.

AUTHOR DECLARATIONS

Conflict of Interest

The author has no conflicts to disclose.

DATA AVAILABILITY

The data that support the findings of this study are available from the corresponding author upon reasonable request.

[1]See Supplementary material at [URL will be inserted by AIP].

[2]See Supplementary material at [URL will be inserted by AIP] for a comparison of the STL of finite PAM with simply supported and clamped boundary conditions.

Cremer, L., Heckl, M., and Petersson, B. A. T. (**2005**). *Structure-Borne Sound: Structural Vibrations and Sound Radiation at Audio Frequencies*, 3 ed. (Springer, Berlin).

Cummer, S. A., Christensen, J., and Alù, A. (**2016**). "Controlling sound with acoustic metamaterials," Nat. Rev. Mater. **1**(3), 16001, doi: 10.1038/natrevmats.2016.1.

Gao, N., Zhang, Z., Deng, J., Guo, X., Cheng, B., and Hou, H. (**2022**). "Acoustic Metamaterials for Noise Reduction: A Review," Adv. Mater. Technol. 2100698, doi: 10.1002/admt.202100698.

Huang, T.-Y., Shen, C., and Jing, Y. (**2016**). "Membrane- and plate-type acoustic metamaterials," J. Acoust. Soc. Am. **139**(6), 3240–3250, doi: 10.1121/1.4950751.

Langfeldt, F., and Gleine, W. (**2019**). "Membrane- and plate-type acoustic metamaterials with elastic unit cell edges," J. Sound Vib. **453**, 65–86, doi: 10.1016/j.jsv.2019.04.018.

Langfeldt, F., and Gleine, W. (**2020**a). "Impact of Manufacturing Inaccuracies on the Acoustic Performance of Sound Insulation Packages with Plate-Like Acoustic Metamaterials," SAE Int. J. Adv. & Curr. Prac. in Mob. **3**(2), 1092–1100, doi: 10.4271/2020-01-1562.

Langfeldt, F., and Gleine, W. (**2020**b). "Optimizing the bandwidth of plate-type acoustic metamaterials," J. Acoust. Soc. Am. **148**(3), 1304–1314, doi: 10.1121/10.0001925.

Ma, F., Huang, M., and Wu, J. H. (**2017**). "Acoustic metamaterials with synergetic coupling," J. Appl. Phys. **122**(21), 215102, doi: 10.1063/1.5003276.

Ma, F., Wang, C., Liu, C., and Wu, J. H. (**2021**). "Structural designs, principles, and applications of thin-walled membrane and plate-type acoustic/elastic metamaterials," J. Appl. Phys. **129**(23), 231103, doi: 10.1063/5.0042132.

Ma, G., and Sheng, P. (**2016**). "Acoustic metamaterials: From local resonances to broad horizons," Sci. Adv. **2**(2), e1501595, doi: 10.1126/sciadv.1501595.

Peiffer, A., Grünewald, M., and Lempereur, P. (**2015**). "Comment on "a lightweight yet sound-proof honeycomb acoustic metamaterial" [Appl. Phys. Lett. 106, 171905 (2015)]," Appl. Phys. Lett. **107**(21), 216101, doi: 10.1063/1.4936237.

Sui, N., Yan, X., Huang, T.-Y., Xu, J., Yuan, F.-G., and Jing, Y. (**2015**). "A lightweight yet sound-proof honeycomb acoustic metamaterial," Appl. Phys. Lett. **106**(17), 171905, doi: 10.1063/1.4919235.

Thompson, D. J., Gardonio, P., and Rohlfing, J. (**2009**). "Can a transmission coefficient be greater than unity?," Appl. Acoust. **70**(5), 681–688, doi: 10.1016/j.apacoust.2008.08.001.

Van Belle, L., Claeys, C., Deckers, E., and Desmet, W. (**2019**). "The acoustic insulation performance of infinite and finite locally resonant metamaterial and phononic crystal plates," MATEC Web Conf. **283**(June), 09003, doi: 10.1051/matecconf/201928309003.

Varanasi, S., Bolton, J. S., and Siegmund, T. (**2017**). "Experiments on the low frequency barrier characteristics of cellular metamaterial panels in a diffuse sound field," J. Acoust. Soc. Am. **141**(1), 602–610, doi: 10.1121/1.4974257.

Varanasi, S., Bolton, J. S., Siegmund, T. H., and Cipra, R. J. (**2013**). "The low frequency performance of metamaterial barriers based on cellular structures," Appl. Acoust. **74**(4), 485–495, doi: 10.1016/j.apacoust.2012.09.008.

Ventsel, E., and Krauthammer, T. (**2001**). *Thin Plates and Shells: Theory, Analysis, and Applications* (Marcel Dekker, New York).

Villot, M., Guigou, C., and Gagliardini, L. (**2001**). "Predicting the Acoustical Radiation of Finite Size Multi-layered Structures by Applying Spatial Windowing on Infinite Structures," J. Sound Vib. **245**(3), 433–455, doi: 10.1006/jsvi.2001.3592.

Wang, X., Chen, Y., Zhou, G., Chen, T., and Ma, F. (**2019**). "Synergetic coupling large-scale plate-type acoustic metamaterial panel for broadband sound insulation," J. Sound Vib. **459**(August), 114867, doi: 10.1016/j.jsv.2019.114867.

Xiao, Y., Cao, J., Wang, S., Guo, J., Wen, J., and Zhang, H. (**2021**). "Sound transmission loss of plate-type metastructures: Semi-analytical modeling, elaborate analysis, and experimental validation," Mech. Syst. Signal Process. **153**, 107487, doi: 10.1016/j.ymssp.2020.107487.

Yang, M., Ma, G., Wu, Y., Yang, Z., and Sheng, P. (**2014**). "Homogenization scheme for acoustic metamaterials," Phys. Rev. B **89**(6), 064309, doi: 10.1103/PhysRevB.89.064309.

Yang, Z., Dai, H. M., Chan, N. H., Ma, G. C., and Sheng, P. (**2010**). "Acoustic metamaterial panels for sound attenuation in the 50–1000 Hz regime," Appl. Phys. Lett. **96**(4), 041906, doi: 10.1063/1.3299007.

Yang, Z., Mei, J., Yang, M., Chan, N. H., and Sheng, P. (**2008**). "Membrane-type acoustic metamaterial with negative dynamic mass," Phys. Rev. Lett. **101**(20), 204301, doi: 10.1103/PhysRevLett.101.204301.